

Louisiana State University LSU Digital Commons

LSU Historical Dissertations and Theses

Graduate School

1977

Cylinder Drag at Low Reynolds Number.

Burke Huner

Louisiana State University and Agricultural & Mechanical College

Follow this and additional works at: https://digitalcommons.lsu.edu/gradschool_disstheses

Recommended Citation

Huner, Burke, "Cylinder Drag at Low Reynolds Number." (1977). *LSU Historical Dissertations and Theses*. 3115.
https://digitalcommons.lsu.edu/gradschool_disstheses/3115

This Dissertation is brought to you for free and open access by the Graduate School at LSU Digital Commons. It has been accepted for inclusion in LSU Historical Dissertations and Theses by an authorized administrator of LSU Digital Commons. For more information, please contact gradetd@lsu.edu.

INFORMATION TO USERS

This material was produced from a microfilm copy of the original document. While the most advanced technological means to photograph and reproduce this document have been used, the quality is heavily dependent upon the quality of the original submitted.

The following explanation of techniques is provided to help you understand markings or patterns which may appear on this reproduction.

- 1. The sign or "target" for pages apparently lacking from the document photographed is "Missing Page(s)". If it was possible to obtain the missing page(s) or section, they are spliced into the film along with adjacent pages. This may have necessitated cutting thru an image and duplicating adjacent pages to insure you complete continuity.**
- 2. When an image on the film is obliterated with a large round black mark, it is an indication that the photographer suspected that the copy may have moved during exposure and thus cause a blurred image. You will find a good image of the page in the adjacent frame.**
- 3. When a map, drawing or chart, etc., was part of the material being photographed the photographer followed a definite method in "sectioning" the material. It is customary to begin photoing at the upper left hand corner of a large sheet and to continue photoing from left to right in equal sections with a small overlap. If necessary, sectioning is continued again — beginning below the first row and continuing on until complete.**
- 4. The majority of users indicate that the textual content is of greatest value, however, a somewhat higher quality reproduction could be made from "photographs" if essential to the understanding of the dissertation. Silver prints of "photographs" may be ordered at additional charge by writing the Order Department, giving the catalog number, title, author and specific pages you wish reproduced.**
- 5. PLEASE NOTE: Some pages may have indistinct print. Filmed as received.**

University Microfilms International

300 North Zeeb Road
Ann Arbor, Michigan 48106 USA
St. John's Road, Tyler's Green
High Wycombe, Bucks, England HP10 8HR

77-28,680

HUNER, Burke, 1948-
CYLINDER DRAG AT LOW REYNOLDS NUMBER.

The Louisiana State University and
Agricultural and Mechanical College,
Ph.D., 1977
Physics, fluid and plasma

Xerox University Microfilms , Ann Arbor, Michigan 48106

CYLINDER DRAG AT LOW REYNOLDS NUMBER

A Dissertation

Submitted to the Graduate Faculty
of the
Louisiana State University and
Agricultural and Mechanical College
in partial fulfillment of the
requirements for the degree of
Doctor of Philosophy

in
The Department of Physics and Astronomy

by
Burke Huner
B.S., Louisiana State University, 1970
M.S., Louisiana State University, 1972
August, 1977

ACKNOWLEDGEMENTS

It is my desire to express thanks to Dr. Robert E. Williams who first suggested this problem and to Dr. Robert G. Hussey for his guidance, encouragement and assistance throughout this investigation. Special thanks are due to Jacqueline Tamas who typed this manuscript and to Nancy P. Harris for doing the figures.

TABLE OF CONTENTS

CHAPTER	Page
I. INTRODUCTION.	1
II. EXPERIMENT.	15
III. RESULTS	29
IV. SUMMARY AND CONCLUSIONS	46
REFERENCES	48
VITA	51

LIST OF FIGURES

Figure	Page
1. The Geometry of the Problem.	1
2. The Drag Coefficient for Spheres	8
3. The Drag Coefficient for Cylinders	9
4. The Fractional Deviation of the Drag from the Stokes Drag for a Sphere	10
5. The Fractional Deviation of the Drag from the Lamb Drag for a Cylinder	12
6. A Schematic Representation of the Apparatus. . .	16
7. The Effect of the Boundaries Parallel to the Cylinder Axis. The Different Symbols, Representing Different Diameters, are the Same as in Fig. 8. The Cylinder Length L is Given for the Longest and Shortest Length of Each Diameter	30
8. An Empirical Correlation of the Data Appearing in Fig. 7.	31
9. The Linear Relation Between $1/U_L$ and $1/L$. The Solid Lines are Least Squares Fits to the Data While the Dashed Lines are Calculated from Shi's Formula.	35
10. An Empirical Correlation of the Data Appearing in Fig. 9. This Figure Also Includes Data for the #65 and #70 Cylinders.	37
11. The Fractional Deviation from the Lamb Drag. The Curve Passing Through the Data is an Empirical Fit. Error Bars are Taken from Table III.	41
12. A Plot of Drag Coefficient Versus Reynolds Number	44
13. The Asymptotic Approach to the Lamb Formula. . .	45

LIST OF TABLES

Table	Page
I. Experimental Parameters and Results.	21
II. Effect of the Sidewall Boundaries.	23
III. Error Summary.	27
IV. Variation of Terminal Velocity with Length . . .	36

ABSTRACT

From terminal velocity measurements of solitary finite length circular cylinders settling in a large rectangular tank of fluid, drag values for infinite length circular cylinders translating at constant speed through an unbounded fluid were obtained. With the Reynolds number defined as $Re = 2aU\rho/\mu$ where $2a$ was the cylinder diameter, ρ was the fluid density, μ the fluid viscosity, and U the speed of translation, the range of Reynolds numbers spanned in this experiment was 0.23 to 2.6. The drag was determined as the effective weight of the cylinder in the liquid and the Reynolds number was determined from the terminal velocity measurements by the time of flight method. Complete data tables are included.

The effects of finite length and finite boundaries were accounted for by empirical corrections. The effects of the container endwalls and bottom were observed to be negligibly small. The sidewalls caused a variation in the terminal velocity proportional to the reciprocal of the wall separation squared. This correction was less than 0.1%. The largest correction was for the finite length. It ranged from 6.6% to 1.4%. When the influence of the side walls was removed, it was found that the reciprocal of the terminal velocity was linearly proportional to the reciprocal of the length.

The final results approach Lamb's solution of the Oseen equations as the Reynolds number decreases. The data are in close agreement with Kaplun's matched asymptotic series solution for Reynolds numbers less than 0.5, and are in excellent accord with the numerical solutions of Takami and Keller at Reynolds numbers of 1 and 2.

CHAPTER I

INTRODUCTION

A. Statement of the Problem

Consider a sphere or an infinite length circular cylinder (for convenience object or obstacle), either of diameter $2a$, immersed in an infinite free stream of homogeneous, incompressible, Newtonian fluid of density ρ and viscosity μ and in the presence of a conservative body force. The free stream is assumed to be uniform far from the origin of a coordinate system which coincides with the center of the object. The x -axis is taken in the direction of the free stream. The geometry of the problem is shown in Fig. 1. The subject of interest in this paper is the

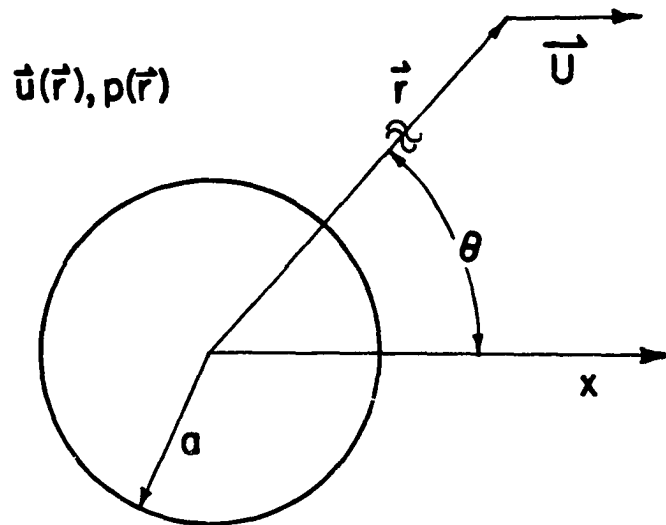


Fig. 1. The geometry of the problem.

determination of the drag (drag per unit length in the case of the cylinder) in terms of $2a$, μ , ρ and the free stream velocity \vec{U} for small values of the Reynolds number

$$Re = 2a|\vec{U}|\rho/\mu.$$

B. Theoretical Investigations

The drag is that part of the total force exerted by the fluid on the sphere or cylinder parallel to the direction of the free stream and is calculated by summing the fluid stresses across the fluid-solid interface once the velocity $\vec{u}(\vec{r})$ and the pressure $p(\vec{r})$ at every point \vec{r} in the fluid are known. $\vec{u}(\vec{r})$ and $p(\vec{r})$ are determined from the steady flow Navier-Stokes equation

$$\rho\vec{u}(\vec{r}) \cdot \nabla\vec{u}(\vec{r}) = -\nabla p(\vec{r}) + \vec{F} + \mu\nabla^2\vec{u}(\vec{r}), \quad (1)$$

mass conservation

$$\nabla \cdot \vec{u}(\vec{r}) = 0, \quad (2)$$

and the boundary conditions

$$\vec{u}(\vec{r}) = 0 \quad \text{on the surface} \quad (3a)$$

$$\vec{u}(\vec{r}) \rightarrow \vec{U} \quad |\vec{r}| \rightarrow \infty \quad (3b)$$

$$p(\vec{r}) - p_0 \rightarrow 0 \quad |\vec{r}| \rightarrow \infty \quad (3c)$$

where \vec{F} is the body force and p_0 is the pressure at $|\vec{r}| = \infty$. \vec{F} has been assumed conservative so it may be expressed as the negative gradient of a scalar function. This allows the pressure and body force terms in Eq. (1) to be combined

begetting some mathematical simplification. This new term is called the modified pressure.

Consider the velocity terms in Eq. (1). The diameter $2a$ and the magnitude of the free stream velocity U are a representative length and speed for the flow field as a whole. It is reasonable that the estimates

$$\rho \vec{u} \cdot \nabla \vec{u} \sim \rho U^2 / 2a \quad (4a)$$

$$\mu \nabla^2 \vec{u} \sim \mu U / (2a)^2 \quad (4b)$$

will have the proper order of magnitude. The ratio of these two estimates, $Re = 2aU\rho/\mu$ is dimensionless and is the previously defined Reynolds number. The Reynolds number is a measure of the importance of inertial forces as compared to viscous forces in computing the velocity and pressure fields. If the inertial forces are negligible compared to the viscous forces (i.e. $Re \ll 1$) then the Navier-Stokes equation can be approximated as

$$0 = -\nabla p(\vec{r}) + \mu \nabla^2 \vec{u}(\vec{r}) \quad (5)$$

where $p(\vec{r})$ is now the modified pressure. Equation (5) is frequently referred to as Stokes' equation because it was Stokes¹ who first used it as an approximation to the full Navier-Stokes equation. The condition necessary for Eq. (5) to be valid is called the Stokes approximation or the condition for creeping flow (or Stokes flow). Stokes successfully solved Eq. (5) for the drag on a sphere and obtained the result

$$D_S = 6\pi\mu Ua \quad (6)$$

where D_S is the sphere drag. He also attempted to solve Eq. (5) for the cylinder drag per unit length but was unable to find a solution for the velocity field which satisfied the boundary conditions. This was interpreted by Stokes to mean that there was no stable flow pattern for the cylinder; experiments, however, showed this conclusion to be incorrect. The non-existence of a solution to the Stokes equations for the steady motion of fluid past a circular cylinder has become known as the Stokes paradox.²

The Stokes paradox remained unresolved for many years until Oseen³ re-examined Stokes' solution for the sphere. From this analysis he deduced that while close to the sphere the Stokes approximation is valid, far from the sphere where the relative fluid motions become small the inertial forces become comparable in magnitude to the viscous forces. Thus, Stokes approximation breaks down far from the sphere and inertia cannot be neglected. (The solution that Stokes found for the sphere neglecting inertia is by Oseen's criticism not a uniformly valid first approximation to the Navier-Stokes equation. The drag deduced from Stokes solution is correct, however, because it is computed at the sphere's surface - where inertia can be neglected.) Oseen proposed to take into account the inertial forces in the region where they are comparable with the viscous forces, but to neglect them close to the

surface by approximating the term $\vec{u}(\vec{r}) \cdot \nabla \vec{u}(\vec{r})$ by $\vec{U} \cdot \nabla \vec{u}(\vec{r})$. This replacement is called Oseen's approximation and the resulting equations are called Oseen's equations.

$$\rho \vec{U} \cdot \nabla \vec{u}(\vec{r}) = -\nabla p(\vec{r}) + \mu \nabla^2 \vec{u}(\vec{r}) \quad (7)$$

where $p(\vec{r})$ is the modified pressure. Oseen solved this equation to obtain the next higher approximation for the Stokes' sphere drag

$$D_0 = 6\pi\mu Ua(1 + \frac{3}{16} \text{Re}) \quad (8)$$

where D_0 is the Oseen drag for the sphere. This result is to be considered fortuitous as Eq. (7) is a valid approximation to the Navier-Stokes equation only to the order of the Reynolds number. Lamb⁴ solved the corresponding cylinder problem to find the cylinder drag per unit length:

$$D_L = 4\pi\mu U\epsilon \quad (9a)$$

where

$$\epsilon = [\frac{1}{2} - \gamma - \ln(\text{Re}/8)]^{-1} \quad (9b)$$

and $\gamma = 0.577216\dots$ is Euler's constant.

To obtain higher order approximations to the Navier-Stokes equation the technique of matched asymptotic expansions^{5,6} has been developed. The flow field surrounding the sphere or cylinder is divided into two regions and separate, locally valid, expansions are developed. The substitution of these expansions in the Navier-Stokes equations will yield a set of differential

equations for the coefficients of the expansions but only one set of physical boundary conditions is applicable to each expansion - the no-slip condition for the inner expansion and the free stream condition for the outer expansion - so that unique solutions cannot be immediately derived. The fact that the two expansions are different forms of the same exact solution and that they must be equal at some intermediate region leads to a procedure which yields further boundary conditions for each expansion. From this matching condition it is possible to determine alternatively successive terms in each expansion - a procedure which in principle can be carried out indefinitely but which in practice often becomes mathematically difficult after a few iterations. Proudman and Pearson⁵ used the method of matched asymptotic expansions to verify Oseen's result for the sphere and to extend the sphere drag to the next higher approximation. They found the sphere drag to be

$$D_P = 6\pi\mu Ua(1 + \frac{3}{16} Re + \frac{9}{160} Re^2 \ln (Re/2)) \quad (10)$$

correct to the order of the Reynolds number squared.

Kaplun⁶ extended Lamb's solution of the cylinder drag per unit length and found

$$D_K = 4\pi\mu U\epsilon(1 - 0.87\epsilon^2) \quad (11)$$

with an error on the order of ϵ^4 .

C. Comparison of Experiments and Theory

The traditional manner of presenting drag measurements and calculations is on a dimensionless plot of drag coefficients, C versus Reynolds number.⁷ C is defined by

$$C = D_T / \frac{1}{2} \rho U^2 A \quad (12)$$

where D_T is the total drag and A is the area of the object projected on the plane normal to \vec{U} . For the sphere $A = \pi a^2$ and for the cylinder $A = 2aL$ where L is the length of the cylinder and $L \rightarrow \infty$. Figure 2 is such a plot for the sphere at small Reynolds number and Fig. 3 is the corresponding plot for the cylinder.

Maxworthy⁸ suggested that this traditional manner of presenting drag results may be inadequate for detailed analysis for small values of the Reynolds number. Considering the drag on a sphere, he showed that a more informative view could be obtained if one plotted the fractional deviation of the sphere drag from the Stokes drag. Figure 4 is such a plot for a sphere. D is the sphere drag and $D_S = 6\pi\mu Ua$ is the Stokes drag. Shown in Fig. 4 are the curves drawn from the normalized formula of Oseen, the formula of Proudman and Pearson, the extension of Proudman and Pearson's solution by Chester and Breach,⁹ and the numerical work of Dennis and Walker¹⁰ who used Van Dyke's¹¹ semi-analytical method of series truncation.

The experimental points of Maxworthy agree well with the more recent measurements of Sutterby.¹² The data agree

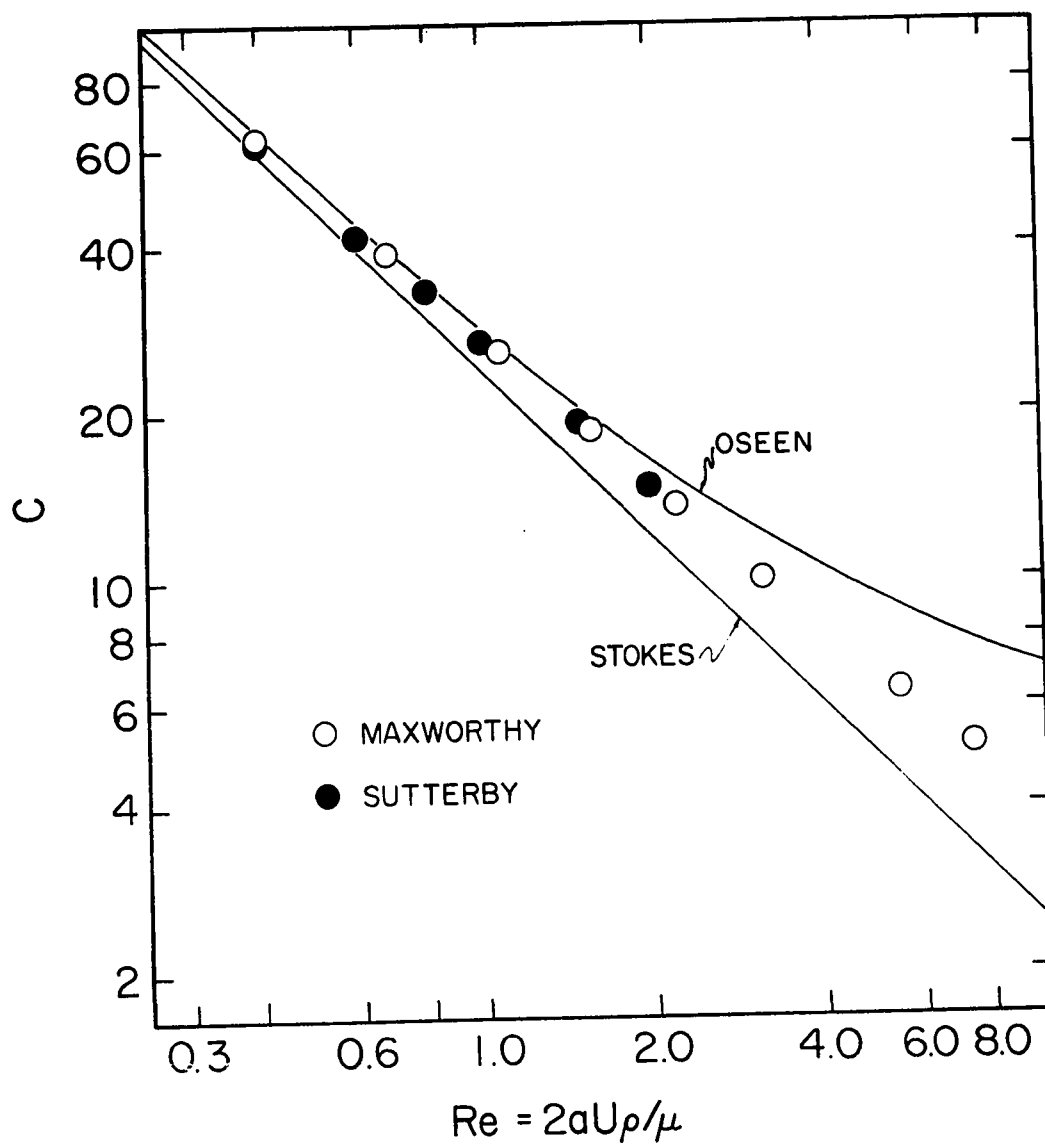


Fig. 2

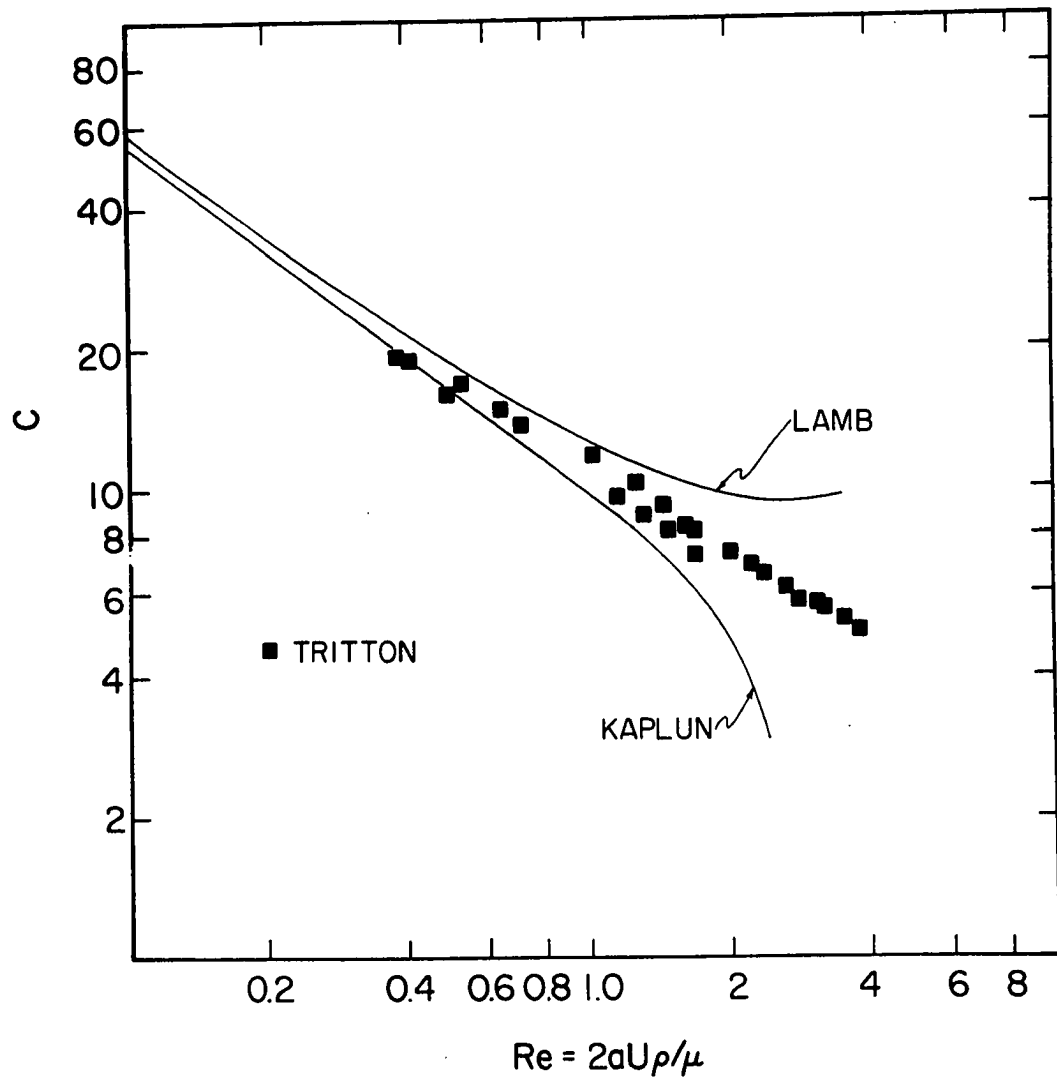


Fig. 3

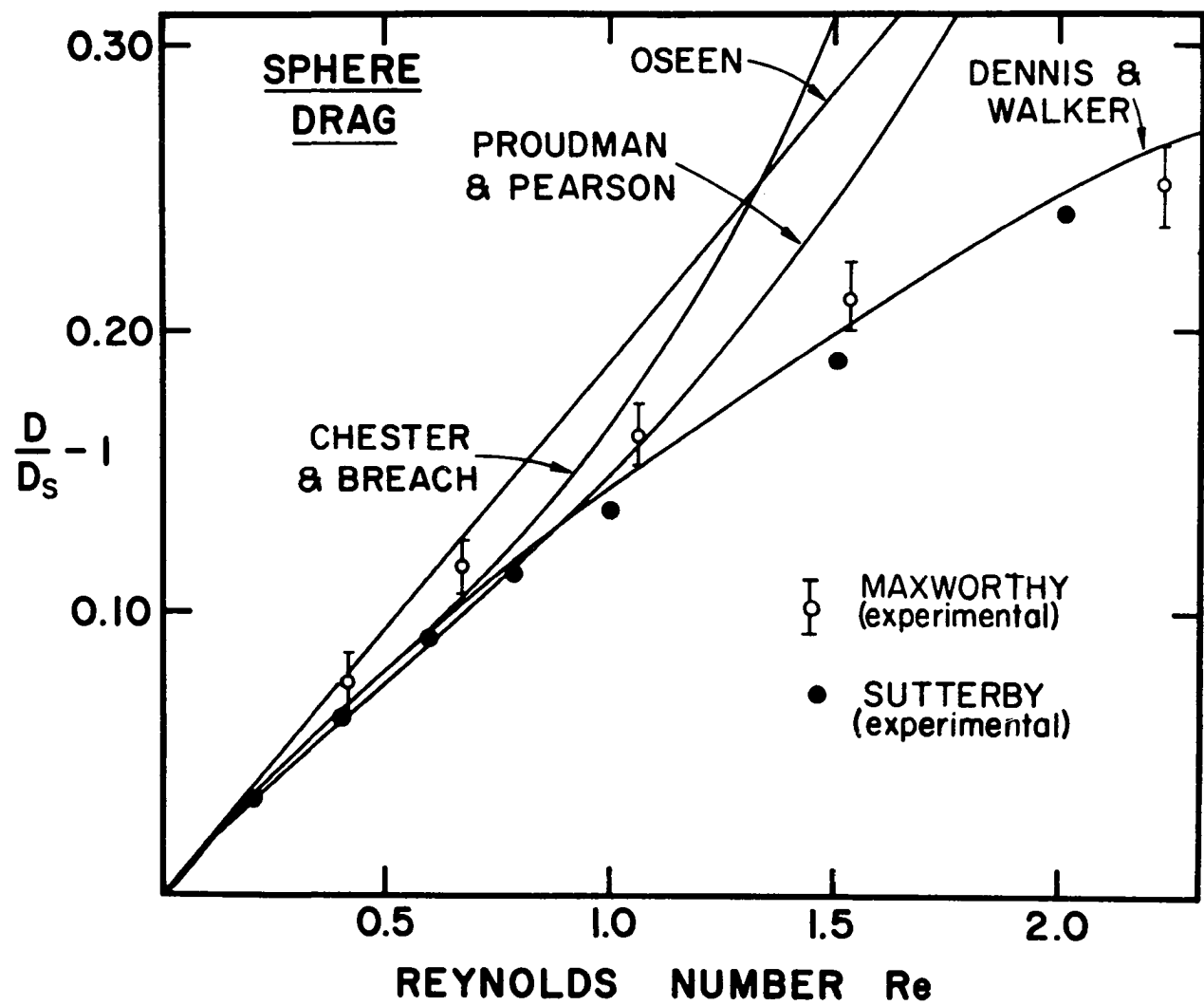


Fig. 4

best with Dennis and Walker's solution at the higher Reynolds number but below $Re = 0.8$ the data agree also with Chester and Breach's solution. For $Re \leq 0.4$ all the different theoretical approaches agree with each other and with experiment. It appears that the results for the low Reynolds number drag on a sphere are well established.

A similar plot for circular cylinders can be made but it will not be precisely analogous to Fig. 4 for two reasons: First, it is the drag per unit length that must be considered and second, because of the Stokes paradox, there is no result for cylinders that corresponds exactly to D_S for spheres. However, for cylinders there is the approximate solution of the Oseen equations due to Lamb that can be used for reference. According to Proudman and Pearson this is the same order of approximation as the Stokes drag for the sphere. Figure 5 results from plotting the fractional deviation of the measured and calculated cylinder drag from Lamb's solution. D is the cylinder drag per unit length and D_L is the Lamb drag per unit length.

The curves shown in Fig. 5 are the matched asymptotic expansion calculation of Kaplun, Underwood's¹³ application of the series truncation method, and a formula proposed by Williams and Hussey.¹⁴ Only a small portion of Tritton's¹⁵ and Jayaweera and Mason's¹⁶ extensive experimental data is shown in Fig. 5. Tritton's measurements extend from $Re = 0.5$ to $Re = 100$ and were made by observing the deflection of

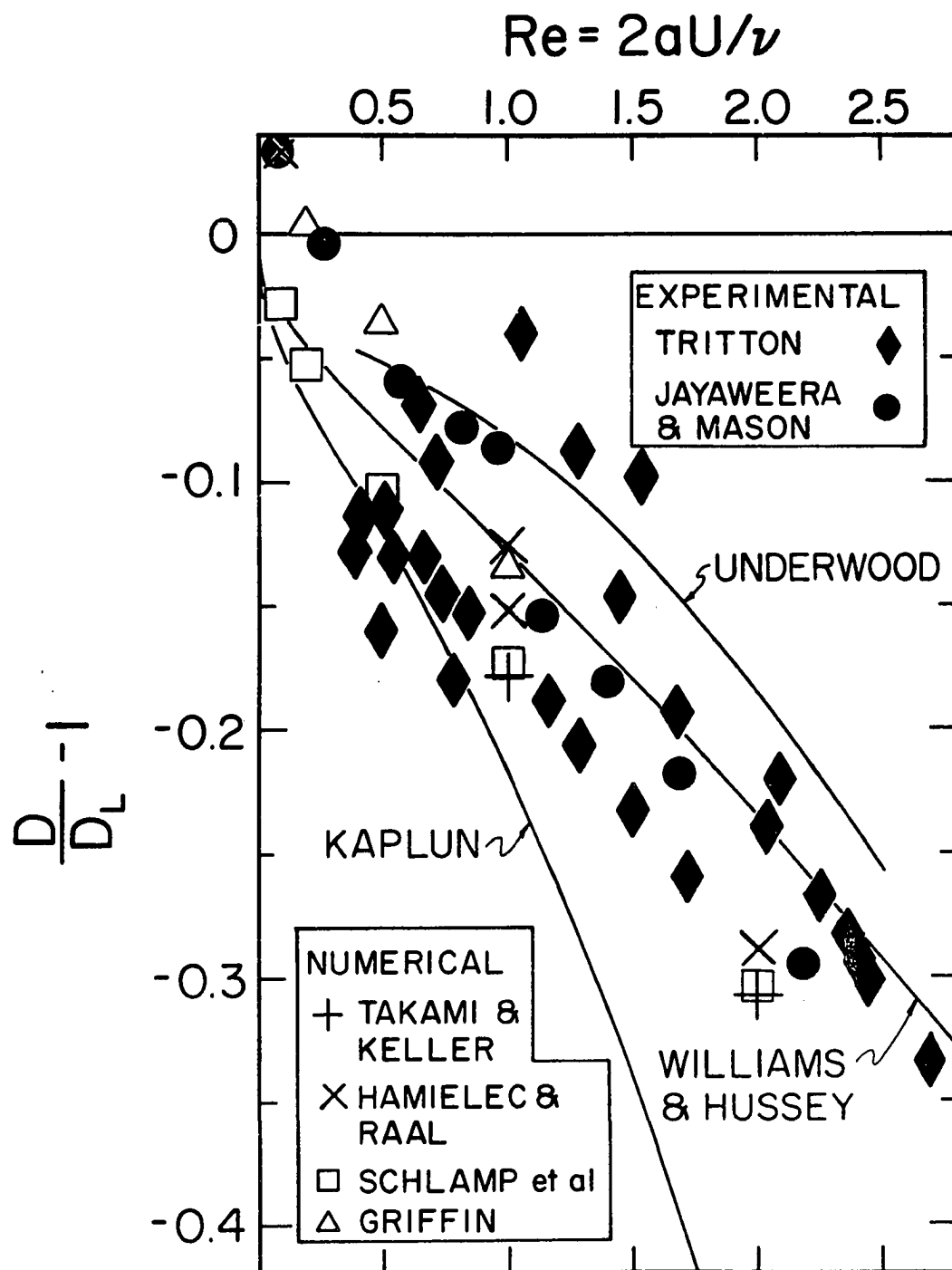


Fig. 5

the free end of a fiber fixed in the test chamber of a wind tunnel. Jayaweera and Mason measured the terminal velocities of rods falling in liquid paraffin to obtain results from $Re = 0.01$ to $Re = 1000$.

Also shown in Fig. 5 are points obtained by various numerical solutions of the full Navier-Stokes equations. The recent work of Schlamp, Pruppacher, and Hamielec,¹⁷ who used computational outer boundaries as large as 1100 radii, agrees well with the results of Takami and Keller,¹⁸ who used an extrapolation technique to eliminate the boundary effect. Not shown but in substantial agreement with these two solutions are the results of Dennis and Shimshoni,¹⁹ who treated a pseudo-Oseen problem, and Nieuwstadt and Keller,²⁰ who also used series truncation but solved the simultaneous equations in a manner different from Underwood. Higher values of $(D/D_L) - 1$ were obtained by Hamielec and Raal²¹ and by Griffin.²² While the experimental results of Tritton and of Jayaweera and Mason are consistent with each other, the scatter of the points in the region of $Re = 1$ is too large for their data to distinguish between the different theoretical and numerical results.

D. Purpose of Present Work.

The present paper reports drag measurements on circular cylinders in the range $0.23 < Re < 2.6$. The data were obtained by measuring the terminal velocities of rods

falling in silicone oils. Empirical corrections were used to account for the effects of finite lengths and finite boundaries. The results indicate that as the Reynolds number becomes small, the Lamb drag is approached from below via Kaplun's formula. The data agree well with the numerical results of Takami and Keller and Schlamp, et al.

CHAPTER II

EXPERIMENT

Suppose the system of the object and the fluid is given a uniform velocity of $-\vec{U}$. This will bring the fluid at infinity to rest while the object will assume a velocity equal but opposite to the velocity that the free stream had before. This superposition of a uniform rectilinear motion on the system can have no dynamic consequences so the drag is the same whether the object is at rest and the fluid flows against it or whether the fluid is at rest and the object is moving uniformly through it. The consequence of this discussion is that the drag can be measured by observing the terminal velocity of a cylinder sedimenting in a large tank of liquid.

Terminal velocity measurements were made photoelectrically by a time of flight technique in a tank of inside dimensions 50.0 cm x 25.8 cm x 30 cm. The tank was filled to a depth of 27 cm with silicone oil and was equipped with movable Plexiglas walls and a false bottom which allowed variation of the width (25.8 cm to 1.30 cm), the length (50.0 cm to 24 cm), and the depth (27 cm to 16 cm).

The timing apparatus is shown in Fig. 6. A cylinder of length L and diameter $2a$ is shown end on as it falls at its terminal velocity U_H . The cylinder is midway between and parallel to the container walls which are separated by

a distance H . After being released 3 cm beneath the fluid surface, the cylinder fell 7 cm before it reached the first of two timing points defined by focused light beams. The beam of a Metrologic Model 410 Laser was expanded to about 1 cm in diameter by a beam expander (A) and then brought to a focus at the midplane of the fall space by a lens (B). The re-expanding beam was collimated by a lens (C), and a right angle prism (D) displaced the beam downward about 5 cm where another lens (E) refocused the beam to the midplane of the fall space. Lenses (B), (C) and (E) were binocular objectives of diameter 35 mm. Two simple lenses (F) were used to focus the re-emerging light onto a photodetector (G). The details of the photodetector electronics are found in Williams' dissertation.²³ As the cylinder fell through the timing point, it acted like a shutter and momentarily blocked the light reaching the photodetector. The resulting voltage pulses from the photodetector were RC coupled to a timer-counter (Hewlett-Packard 5326B) and were used to control the start-stop gating. Times of flight were measured to 0.01 ms; they ranged from 360 ms to 1200 ms and were reproducible to 0.1% provided that readings were not taken more often than once every two minutes.

Forward scattering from the laser beam was intense enough to observe the beam at the focal points to be less than 0.1 mm in diameter. The back scatter from the laser beam was not of sufficient intensity to allow both focal

points to be observed from the same side of the tank. To make both focal points visible simultaneously, a contact print of a ground glass galvanometer scale was made on 135 mm roll film, and the print was suspended vertically through both focal points. The separation of the focal points was then determined with a cathetometer to an estimated ± 0.05 mm. From the measured spacing and the time of flight, U_H was calculated to an accuracy of 0.2%.

Figure 6 also shows the forces acting on the cylinder. Since the cylinder is falling at its terminal velocity, the drag F is equal to the difference between the weight W and the buoyant force B . The drag per unit length is $D = F/L = (W-B)/L$. In this experiment F was determined by a static weighing of the cylinder in a sample of the fluid in which it was to fall instead of calculating it from the measured cylinder dimensions, the cylinder mass, and the fluid density. The fractional deviation from the Lamb drag is

$$\frac{D}{D_L} - 1 = \frac{F/L}{4\pi\mu U\epsilon} - 1. \quad (13)$$

In this expression, the cylinder diameter enters only through the $\ln(Re/8)$ term in ϵ . In the range of Re in this experiment, $\ln(Re/8)$ is a slowly varying function, so when F is measured directly, Eq. (13) will be relatively insensitive to errors in the measurement of diameter. This is

particularly important for cylinders of small diameter. At the lowest Re in this experiment the error in $(D/D_L)-1$ due to uncertainty in the cylinder diameter was a factor of 1.96 larger for the indirect calculation of F than for the direct measurement of F . The direct measurement of F also suppressed errors in the measurement of length and of the fluid density. Some of this improved accuracy was lost, however, because twice as many weighing operations were necessary to determine F directly. Calculation of the total error in $(D/D_L)-1$ showed that there was a 0.5% advantage in directly measuring F at $Re = 2.6$ and a 1.4% advantage at $Re = 0.23$.

The effective weight ($W-B$) was determined as the product of the effective mass m' and the local value of the gravitational acceleration g (979.35 cm/sec^2). An analytical balance accurate to $\pm 0.1 \text{ mg}$ was used to measure the effective masses. In this measurement, the cylinders were suspended from a thin wire carriage. Since it was necessary to measure the effective mass of the carriage, the overall uncertainty in the effective mass of the cylinders was $\pm 0.2 \text{ mg}$. Values of the effective masses ranged from 225.6 mg for the largest diameter, longest cylinder to 11.9 mg for the smallest diameter, shortest cylinder. On the average, the measured effective masses were larger than the calculated effective masses by 0.4%. Differences of $\pm 4\%$ were noted for the smallest cylinders.

The cylinders were made from HSS drill blanks (American Standard Twist Drill nomenclature sizes #61 through #75). The diameters ranged from 0.0982 cm (#61) to 0.0526 cm (#75). Dimensions of the cylinders are given in Tables I and II. Various lengths were used for the sizes #61, 65, 70, and 75; single lengths were used for the other sizes. The ends of the cylinders were ground square (i.e., flat and perpendicular to the axis). Lengths were measured to ± 0.001 " with a traveling microscope and diameters were measured with micrometer calipers to ± 0.0001 ".

Two silicone oils were used. The first was General Electric 0.5 cm²/sec liquid (SF96) and the second was a 1 cm²/sec blend of SF96 and Dow Corning 5 cm²/sec liquid (DC710). These fluids are known to be Newtonian at the low shear rates of this experiment.²⁴ Viscosities were determined with Cannon-Fenske routine viscometers immersed in a controlled temperature bath over the temperature range 19 to 26°C. Fluid densities were determined over the same temperature range by measuring the buoyant force on a mass of known volume. As compared to other fluids commonly used in experiments of this type, the silicone oils have lower temperature coefficients of viscosity. For example, the 1 cm²/sec fluid had a temperature coefficient of viscosity $\alpha = \nu^{-1}(d\nu/dT) = 2.0 \times 10^{-2}(\text{°C})^{-1}$ at 23°C. Glycerine-water mixtures and petroleum oils of the same viscosity have temperature coefficients of $7.0 \times 10^{-2}(\text{°C})^{-1}$ and

Table I. Experimental Parameters and Results

Rod #	2a cm	L cm	D dyn/cm	ν cm ² /sec	ρ_L g/cm ³	U_H cm/sec	U cm/sec	Re	$1-(D/D_L)$
61	0.09819	4.196	51.91	0.5240	0.9571	13.827	14.068 (14.025)	2.636	0.395
62	0.09477	3.812	47.79	0.5277	0.9576	12.998	13.255	2.380	0.356
63	0.09317	3.830	46.31	0.5277	0.9576	12.751	13.004	2.296	0.343
64	0.09025	3.830	43.76	0.5277	0.9576	12.370	12.617	2.158	0.326
65	0.08864	3.851	42.55	0.5277	0.9576	12.219	12.373 (12.432)	2.078	0.312
66	0.08285	3.437	40.70	0.5277	0.9576	12.015	12.278	1.928	0.297
67	0.08079	3.514	35.60	0.5277	0.9576	10.982	11.228	1.719	0.271
68	0.07752	3.569	32.15	0.5277	0.9576	10.304	10.537	1.548	0.248
69	0.07332	3.442	28.59	0.5277	0.9576	9.584	9.814	1.364	0.224
70	0.07050	3.233	26.74	0.5280	0.9576	9.209	9.447 (9.395)	1.261	0.211
71	0.06510	3.236	22.51	0.5277	0.9576	8.265	8.486	1.0469	0.183
72	0.06281	2.939	20.95	0.5277	0.9576	7.893	8.128	0.9675	0.174
73	0.05969	2.873	21.30	0.5277	0.9576	8.085	8.323	0.9415	0.169
74	0.05618	2.578	17.28	0.5277	0.9576	7.012	7.257	0.7726	0.152
75	0.05256	2.570	14.66	0.5290	0.9578	6.290	6.520 (6.561)	0.6479	0.140

Table I (continued)

Rod #	2a cm	L cm	D dyn/cm	ν cm ² /sec	ρ_L g/cm ³	U_H cm/sec	U cm/sec	Re	$1-(D/D_L)$
61	0.09819	4.196	51.89	1.0370	0.9623	9.962	10.288 (10.287)	0.9741	0.184
62	0.09477	3.812	47.86	1.0265	0.9620	9.394	9.737	0.8989	0.165
63	0.09317	3.830	46.28	1.0265	0.9620	9.201	9.538	0.8657	0.161
64	0.09025	3.830	43.89	1.0265	0.9620	8.881	9.209	0.8097	0.150
65	0.08864	3.851	42.55	1.0370	0.9623	8.724	9.048 (9.066)	0.7734	0.153
66	0.08285	3.437	40.68	1.0265	0.9620	8.512	8.859	0.7150	0.135
67	0.08079	3.514	35.58	1.0265	0.9620	7.765	8.090	0.6367	0.130
68	0.07752	3.569	32.14	1.0265	0.9620	7.237	7.544	0.5697	0.119
69	0.07332	3.442	28.57	1.0265	0.9620	6.683	6.985	0.4989	0.111
70	0.07050	3.233	26.78	1.0168	0.9611	6.411	6.720 (6.717)	0.4659	0.1024
71	0.06510	3.236	22.50	1.0265	0.9611	5.665	5.953	0.3775	0.0926
72	0.06281	2.939	20.94	1.0265	0.9611	5.355	5.659	0.3463	0.0859
73	0.05969	2.873	21.29	1.0265	0.9611	5.493	5.802	0.3374	0.0858
74	0.05618	2.578	17.27	1.0265	0.9611	4.696	5.011	0.2742	0.0837
75	0.05256	2.570	14.81	1.0370	0.9623	4.190	4.487 (4.438)	0.2274	0.0832

Table II. Effect of the Sidewall Boundaries

 $\rho_L = 0.9623 \text{ g/cm}^3$ and $\nu = 1.039 \text{ cm}^2/\text{sec}$

Rod #	$2a$ (cm)	L (cm)	U_H (cm/s)					
			$H=1.30\text{cm}$	$H=2.00\text{cm}$	$H=4.86\text{cm}$	$H=11.70\text{cm}$	$H=22.46\text{cm}$	$H=25.8\text{cm}$
61	0.09819	1.128	8.356	8.853	9.079	9.106	9.119	9.150
		1.670	8.487	9.123	9.438	9.499	9.484	9.504
		1.966	8.511	9.136	9.527	9.579	9.576	9.622
		2.445	8.452	9.169	9.607	9.673	9.675	9.693
		4.196	8.397	9.238	9.815	9.940	9.935	9.952
65	0.08864	0.833	7.164	7.479	7.716	7.747	7.784	7.773
		1.345	7.393	7.907	8.179	8.223	8.222	8.225
		1.755	7.436	8.027	8.366	8.395	8.409	8.426
		2.433	7.426	8.084	8.491	8.575	8.570	8.571
		3.851	7.292	8.048	8.608	8.691	8.696	8.715

Table II (continued)

Rod #	$2a$ (cm)	L (cm)	U_H (cm/s)					
			$H=1.30\text{ cm}$	$H=2.00\text{ cm}$	$H=4.86\text{ cm}$	$H=11.70\text{ cm}$	$H=22.46\text{ cm}$	$H=25.8\text{ cm}$
70	0.07050	0.729	4.938	5.229	5.374	5.397	5.384	5.376
		1.289	5.209	5.623	5.864	5.906	5.890	5.859
		1.544	5.253	5.699	5.988	6.005	6.027	5.979
		2.019	5.267	5.746	6.067	6.097	6.116	6.070
		3.233	5.189	5.778	6.240	6.289	6.315	6.269
75	0.05256	0.747	3.211	3.455	3.561	3.604	3.603	3.616
		1.0998	3.309	3.593	3.787	3.788	3.795	3.805
		1.433	3.322	3.659	3.898	3.901	3.899	3.923
		1.786	3.372	3.726	4.008	4.027	4.036	4.052
		2.570	3.346	3.788	4.110	4.164	4.164	4.186

$4.6 \times 10^{-2}(\text{°C})^{-1}$ respectively. To achieve a precision of 0.1% or better in viscosity, the temperature need be known to only 0.05°C for the silicone oils. The temperature in the fall space was measured with a mercury-in-glass thermometer having 0.05°C divisions.

There was no temperature regulation of the fluid in the fall space of the container. Before each experiment the fluid was stirred manually and it received stirring periodically throughout the experiment because of the cylinder retrieval operations. During an experimental run, there was a slow warming trend of the fluid (about 0.5°C/3 hours). This drift was not due to localized heating from the laser beam because the beam was blocked except for the short interval of time necessary to make the timing measurement. The temperature drift was independent of the time of day and was probably due to the presence of the experimenter. The correction to F was less than 0.1% and was ignored. The terminal velocity U_H was observed to depend upon the temperature through the temperature dependence of the viscosity. U_H was found to vary accurately as $\nu^{-1/2}$ and this relation was used to adjust the velocities to the same temperature by means of the equation

$$U_H(T_0) = U_H(T) / [1 - \frac{1}{2}\alpha(T-T_0)] \quad (14)$$

where T is the temperature at which the measurement was made and T_0 is the reference temperature (usually the

average temperature for the run); α was evaluated at T_0 . Since the temperature drift was small, the resulting adjustment in the velocity was also small ($<0.3\%$).

Error estimates are summarized in Table III. These estimates are for the longest cylinders of sizes #61 and #75 and for two different viscosities. Errors in the measurement of cylinder length and fluid density were less than 0.1% . The largest source of error was in the measurement of terminal velocity U . The error estimate given for U includes the effect of extrapolating to infinite length (as described subsequently). While the reproducibility of the viscosity measurements was better than 0.1% , the absolute viscosity is known to only 0.25% because of uncertainty in the standard of viscosity.²⁵ The last three columns in Table III give the errors in Reynolds number, the dimensionless drag D/D_L , and the fractional deviation from the Lamb drag, as calculated from the errors in the measured quantities.

Several different methods were used to hold and release the cylinders in the fluid: a mechanical device consisting of a horizontal Plexiglas cylinder with axial grooves on its periphery (similar in form to a tooth-pick dispenser); an electromagnet; and holding the cylinder at its midpoint with tweezers. The results were independent of the method of release. Before each experiment, the cylinders and any ferrous objects that were to be used to

Table III. Error Summary

Rod	Percentage Error								
	Re	$1-(D/D_L)$	m'	U	a	v	Re	(D/D_L)	$1-(D/D_L)$
61	2.636	0.395	0.09	0.35	0.52	0.25	0.67	0.99	1.5
61	0.9741	0.184	0.09	0.67	0.52	0.25	0.88	1.10	4.9
75	0.6479	0.140	0.50	0.88	0.97	0.25	1.33	1.44	8.9
75	0.2274	0.0832	0.50	1.22	0.97	0.25	1.58	1.70	18.8

handle the cylinders were passed through a degaussing coil. Usually cylinders of the same diameter were dropped in order of decreasing length. Altering the dropping order (that is, progressing from shortest to longest length or alternating different diameter cylinders) had no significance. When about ten cylinders had accumulated on the bottom of the tank, retrieval was done with a 1/8" diameter plastic rod which had a slot cut in one end. It could be slipped (like a clothespin) over the waist of the cylinder, pinching it and allowing retrieval without damaging or magnetizing the cylinders.

CHAPTER III

RESULTS

U_H has been defined as the terminal velocity of a cylinder of length L falling midway between and parallel to plane boundaries separated by a distance H . Let U_L be defined as the velocity of a finite length cylinder in an unbounded fluid and let U remain the velocity of an infinite length cylinder in an unbounded fluid. Empirical boundary and length corrections were obtained and were used to calculate U from the measurement of U_H .

A. The Boundary Correction

For the range of Reynolds numbers studied in this experiment, the influence of the container boundaries on U_H was very small. The major boundary influence was that of the sidewalls (i.e., the vertical walls parallel to the axis of the cylinder). The effect of the sidewalls was studied in the $1 \text{ cm}^2/\text{sec}$ fluid with the #61, 65, 70 and 75 cylinders of various length. As H was reduced from 25.8 cm to 1.30 cm, the velocity U_H decreased. The results are given in Table II and in Figs. 7 and 8. In Fig. 7, $4\pi\mu U_H/D$ is plotted against $\log (H/2a)$. As H is reduced, the data tend toward the empirical curve of White,²⁶ who studied the case of boundary dominated flow. Also shown in Fig. 7 is

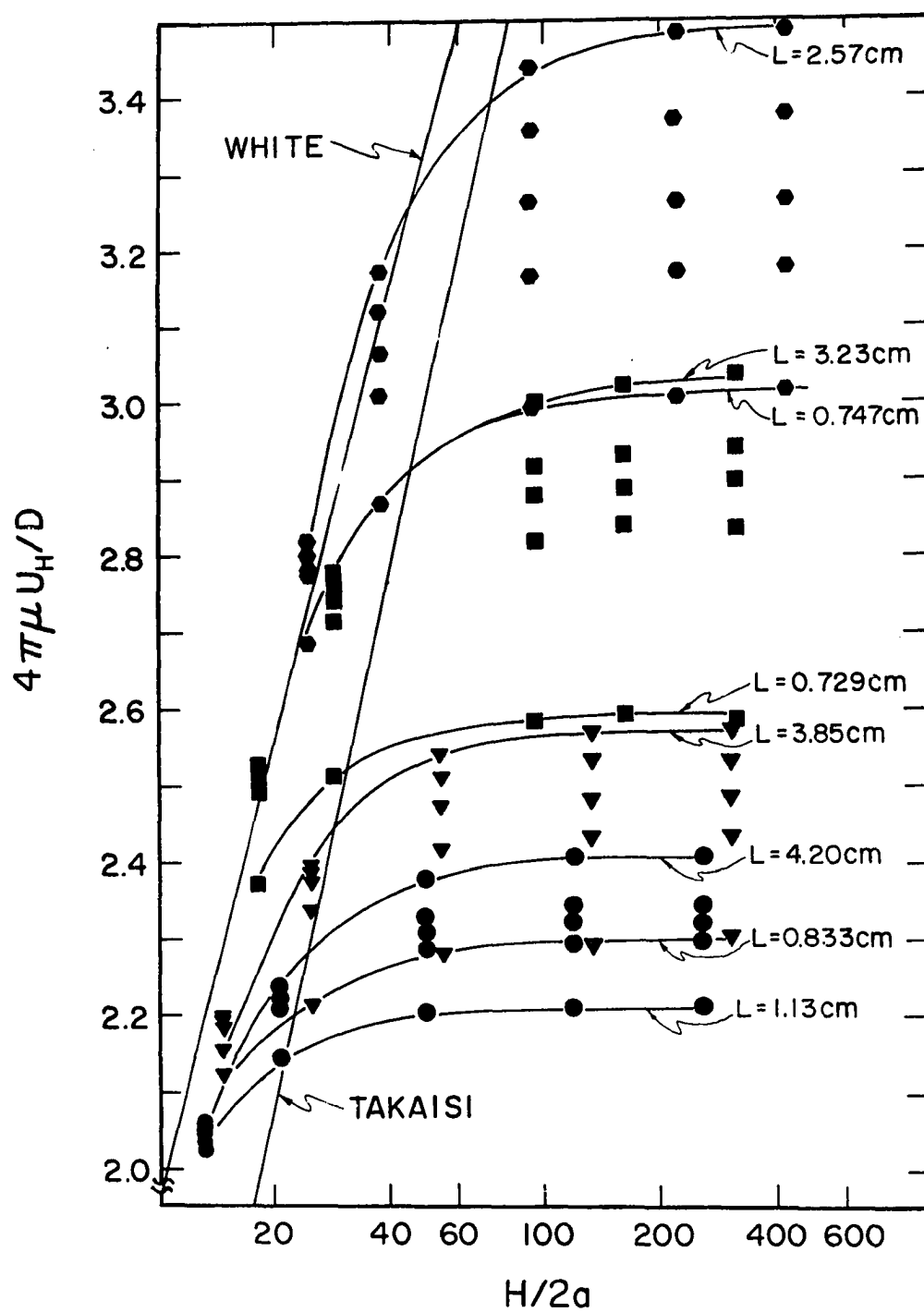


Fig. 7

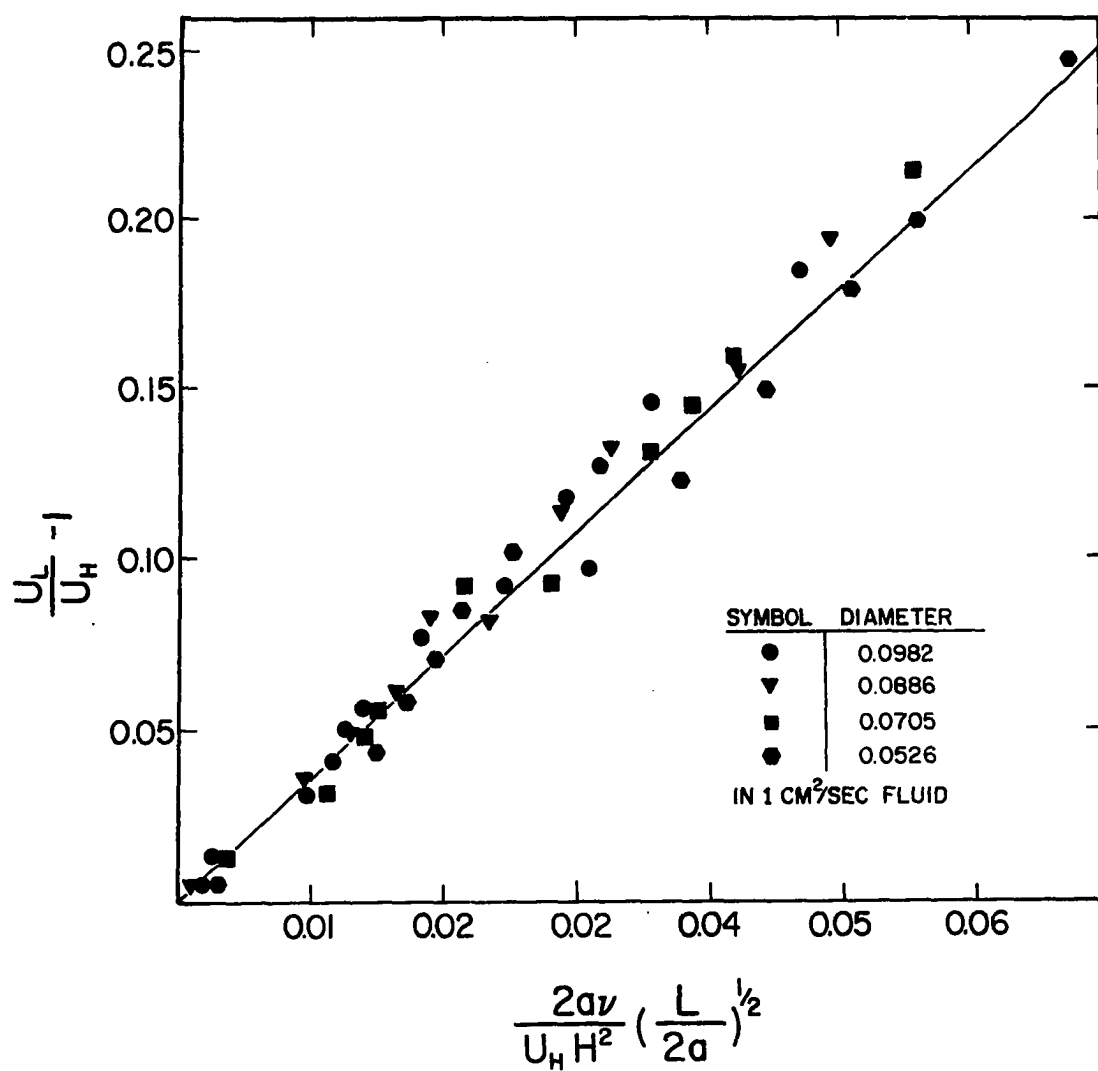


Fig. 8

the theoretical formula of Takaisi,²⁷ who solved Oseen's equations for the drag per unit length of an infinite length cylinder between parallel walls.

When the sidewall influence was small, the reciprocal of U_H was found to vary linearly with $1/H^2$. U_L was obtained by plotting $1/U_H$ versus $1/H^2$ and extrapolating to infinite H . Figure 8 is an empirical correlation of the data; the solid line, which is a least squares fit with zero intercept, is given by

$$U_L/U_H = 1 + 3.60 (2a/H)^2 (L/2a)^{1/2} / Re_H. \quad (15)$$

Therefore, the boundary correction depends not only on the relative distance $H/2a$ but also on the length to diameter ratio $L/2a$ and on the Reynolds number $Re_H = 2aU_H/\nu$. For $Re_H = 1$ and $L/2a = 100$ the boundary correction can be made less than 0.1% by choosing H to exceed 200 diameters. Boundary effects become more important at lower Re_H and longer cylinder lengths. It is clear from Fig. 7 and from the data of White²⁶ and deMestre²⁸ that Eq. (15) is valid only when the boundary influence is small.

Equation (15) can be put into an alternate form:

$$U_L/U_H = 1 + 3.60(1/R_H)(2aL)^{1/2}/H \quad (16)$$

where $R_H = U_H H/\nu$ is a Reynolds number based on boundary separation. If $(2aL)^{1/2}$ is interpreted as the diameter of an equivalent sphere, this correction is (except for the

factor of R_H^{-1}) similar to the corrections derived by Brenner.²⁹

The effects of the bottom and of the endwalls (i.e., the vertical walls perpendicular to the cylinder axis) were observed to be negligibly small. The influence of the bottom was studied with a 0.0337 cm diameter, 1.946 cm length cylinder (ASTD #80) in the 0.5 cm²/sec fluid ($Re_H = 0.24$). Time of flight measurements were made with $H = 25.8$ cm, with the end walls 24 cm from the cylinder ends, and with the bottom of the container 12.11 cm below the lower timing point. Moving the bottom to 6.45 cm below the lower timing point had no detectable influence on the time of flight within the precision of the measurement (0.1%). Moving the bottom to 1.21 cm below the lower timing point resulted in a 0.4% increase in the time of flight. The same cylinder was used to see if the end walls affected U_H . When the container length was halved, there was no change observed in the time of flight within 0.1%. The effect of the free surface was not studied but was presumed to be similar in magnitude to the bottom effect and was therefore neglected.

B. The Length Correction

By far the most important correction was for the effect of the finite length of the cylinders. Experiments were

done in both the $0.5 \text{ cm}^2/\text{sec}$ and $1 \text{ cm}^2/\text{sec}$ fluids with different lengths of the #61, 65, 70, and 75 cylinders. A linear relation was found between $1/U_L$ and $1/L$. This is shown as the solid curve in Fig. 9, and numerical values are given in Table IV. U was obtained by extrapolating to infinite L . The differences between U and U_L for the longest cylinder was 1.4% of U at $Re = 2.6$ and 5.5% of U at $Re = 0.22$. The values of U_H in Table IV were obtained with $H = 25.8 \text{ cm}$.

Figure 10 is a correlation of the data appearing in Fig. 9 and also includes data for the #65 and #70 cylinders. The solid line in Fig. 10 is a least squares fit with zero intercept and is given by

$$U/U_L = 1 + 1.36(2a/L)(Re^{-5/8}). \quad (17)$$

The correction for finite length is more important for cylinders of small length to diameter ratio and at lower Re . With this correction it was possible to obtain U_L for a single cylinder and correct it to U . This was done for the remaining cylinders. The internal consistency of Eq. (17) was examined by applying it to the longest length #61, 65, 70, and 75 cylinders. On the average there was agreement within 0.4% between the value of U obtained by extrapolation from the data and the value calculated from Eq. (17). The maximum disagreement was found at $Re = 0.227$, where it was 1.1%.

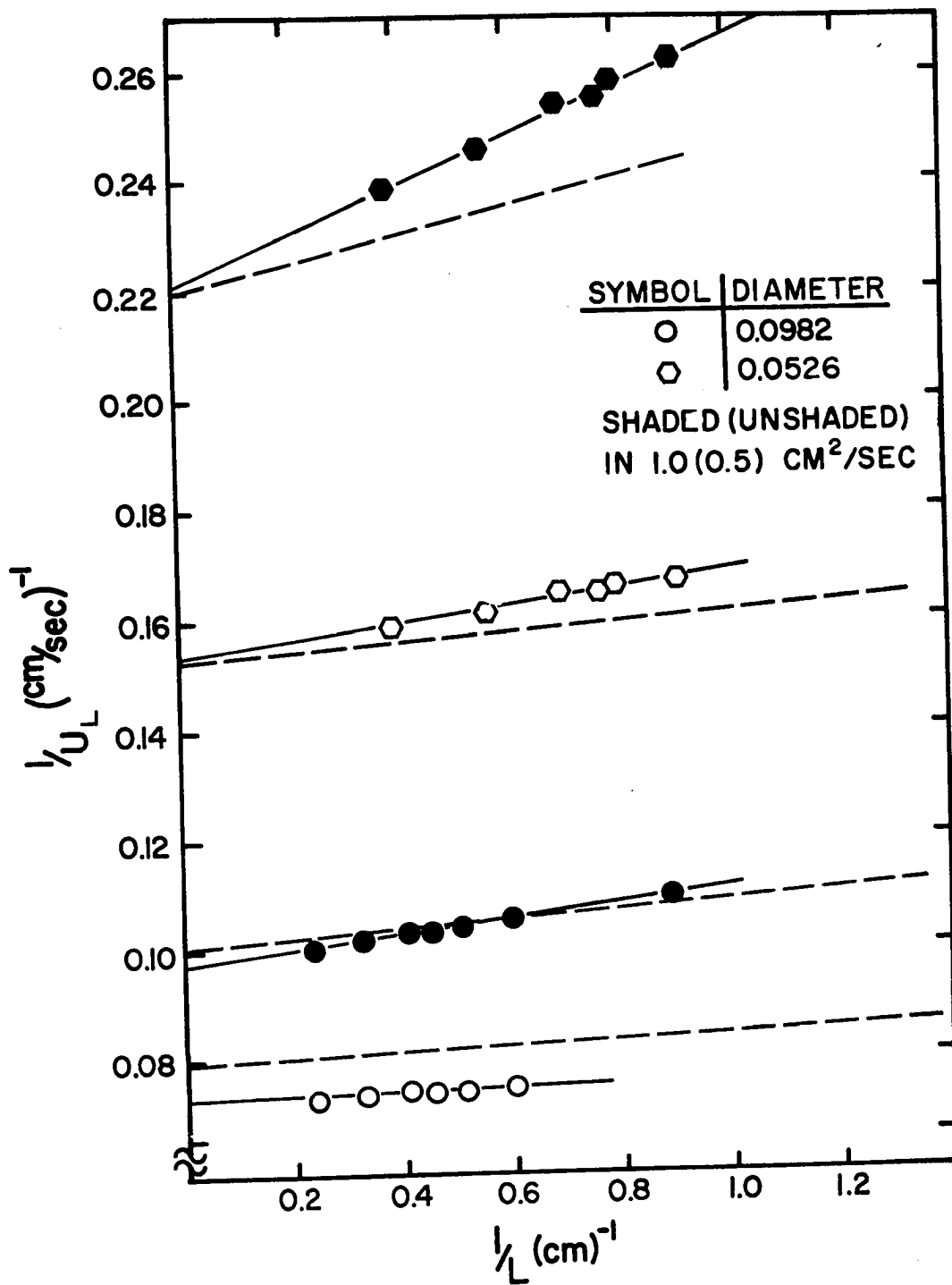


Fig. 9

Table IV. Variation of Terminal Velocity with Length

Rod	2a (cm)	L (cm)	$\nu = 0.524 \text{ cm}^2/\text{sec}$		$\nu = 1.037 \text{ cm}^2/\text{sec}$	
			U_H (cm/sec)	U_L (cm/sec)	U_H (cm/sec)	U_L (cm/sec)
61	0.09819	1.128			9.159	9.161
		1.670	13.493	13.494	9.154	9.516
		1.966	13.557	13.558	9.631	9.633
		2.217	13.639	13.640	9.725	9.728
		2.445	13.605	13.606	9.703	9.706
		3.040	13.706	13.708	9.818	9.821
		4.196	13.827	13.829	9.962	9.966
		∞		14.025		10.287
75	0.05256	0.747			3.620	3.621
		1.0998	5.977	5.978	3.809	3.810
		1.257	6.019	6.020	3.870	3.871
		1.305	6.069	6.070	3.909	3.910
		1.433	6.059	6.060	3.927	3.929
		1.786	6.202	6.203	4.056	4.058
		2.570	6.290	6.291	4.190	4.192
		∞		6.561		4.438

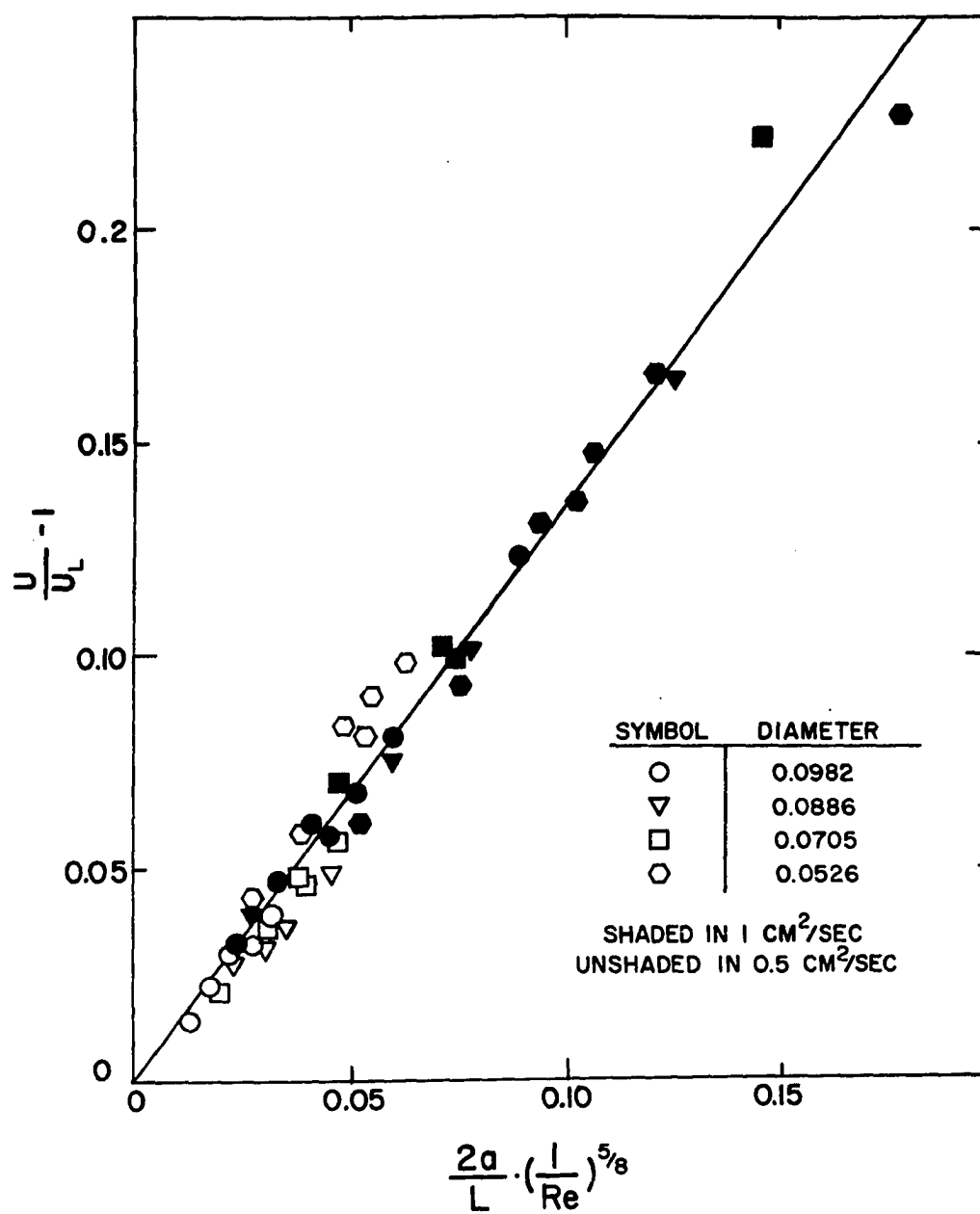


Fig. 10

The data of Jayaweera and Mason¹⁶ are consistent with the linear relation between $1/U_L$ and $1/L$. White²⁶ found a similar but more complicated relation that included the influence of a cylindrical boundary. Furthermore, this extrapolation to infinite length is not without theoretical justification. Shi³⁰ has applied the method of matched asymptotic expansions to a long thin ellipsoid of revolution in transverse flow. He found the drag at low Re to be represented by

$$F/4\pi\mu U_L L = \epsilon + \epsilon^2 [E_1(R/2) + \ln 2 - 1 + 2(1 - e^{-\frac{1}{2}R})/R] + O(\epsilon^3) \quad (18)$$

where L is the major axis, $E_1(x) = \int_x^\infty u^{-1} e^{-u} du$, $R = U_L L/\nu$ and ϵ is the same as our Eq. (9) with $Re = 2aU_L/\nu$ based on the minor axis. For $R > 6$ Eq. (18) can be accurately approximated by

$$F/4\pi\mu U_L L = \epsilon + \epsilon^2 [(2/R) + \ln 2 - 1]. \quad (19)$$

If Eq. (19) is solved by iteration for U_L as a function of L , a linear relation between $1/U_L$ and $1/L$ similar to the present result is found. This is shown as the dashed line in Fig. 9. As can be seen, the general trend of the cylinder data is reproduced by Shi's formula. The agreement cannot be exact because the coefficient of the ϵ^2 term does not vanish in the limit of infinite R (infinite L) as it must if Eq. (19) is to agree with Kaplun's formula for the

cylinder. The difference in the formulas is due to the difference in geometry between the cylinder and the ellipsoid.³⁰

A simple phenomenological model can be developed for the length effect if it is supposed, as Shi has done for the ellipsoid, that the effects of the ends can be isolated from the central section. Let the flow be two dimensional over most of the length of the cylinder and let three dimensional flow be limited to a narrow region (of length Δ) near each end. The drag is considered to consist of the sum of two parts: the drag on the middle, F_m , assumed to be proportional to U_L and L , and the drag on the ends, F_e , assumed to be proportional to U_L and to Δ , but to be independent of L . By assumption, $F_m = k_m U_L L$ and $F_e = k_e U_L \Delta$ where k_m and k_e are constants of proportionality. If $\Delta \ll L$, then the total drag is given by $k_m U_L L + k_e U_L \Delta = \pi a^2 L g(\rho - \rho_L)$ where ρ is the cylinder density and ρ_L is the liquid density. This relation can be solved for $1/U_L$:

$$\frac{1}{U_L} = \frac{k_m}{\pi a^2 g(\rho - \rho_L)} + \frac{k_e \Delta}{\pi a^2 g(\rho - \rho_L)} \frac{1}{L}. \quad (20)$$

Therefore, the linear relation between $1/U_L$ and $1/L$ follows from simple assumptions, primarily that the end effects are small.

C. The Drag

Table I summarizes the results of this experiment. In columns 2 through 4 are the cylinder diameter, the longest cylinder length, and the measured drag per unit length. Columns 5 and 6 give the fluid kinematic viscosity and density. The values of U_H in column 7 are averages of at least 10 trials with $H = 25.8$ cm. U (column 8) was calculated from U_H in two steps by means of Eq. (15) and (17); U_H was first corrected to infinite container by Eq. (5) to get U_L ; then U was determined by solving Eq. (17) by iteration. Column 8 also gives (in parenthesis) the values of U for the #61, 65, 70, and 75 cylinders determined by extrapolation of the data for each cylinder individually. Columns 9 and 10 are the final results. They give the Reynolds number and the fractional deviation from the Lamb drag. The values from these columns are plotted in Fig. 11.

The present results indicate that the Lamb drag is being approached from below via Kaplun's formula. They give good support to the work of Takami and Keller¹⁸ at Reynolds numbers of 1 and 2 (and hence with Nieuwstadt and Keller²⁰ at Reynolds number of 1) and with the more recent work of Schlamp, Pruppacher, and Hamielec.¹⁷ They show a progressive deviation from the values of Hamielec and Raal and of Griffin as the Reynolds number becomes smaller than unity. The present results do not support Underwood's¹³ solution. Nieuwstadt and Keller²⁰ studied the effect of

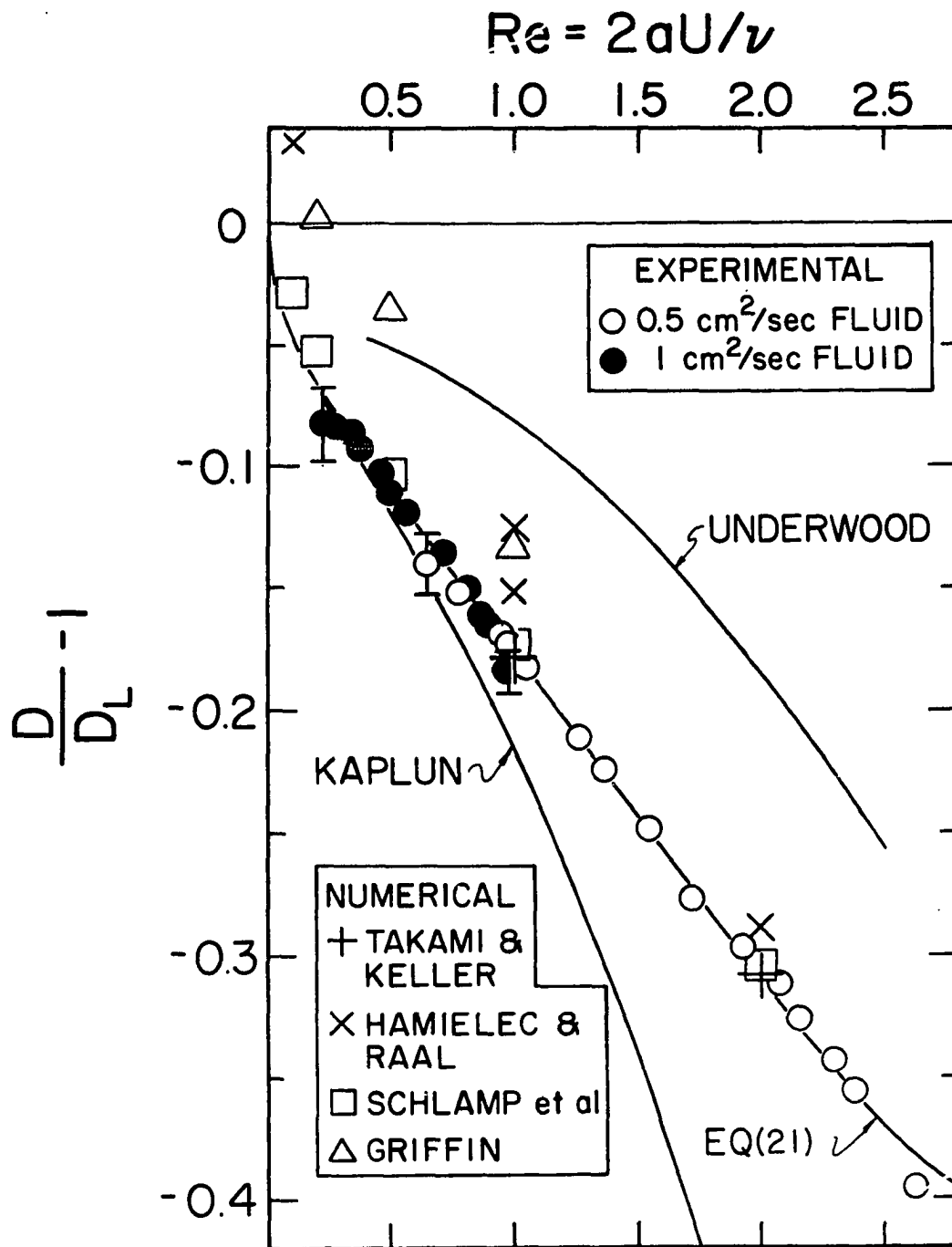


Fig. 11

early series truncation on the accuracy of their solution. They imply that the discrepancy between their (and therefore the present experimental) results and Underwood's results is due to truncation and computational boundaries. The distinguishing factor of the remaining numerical solutions is the management of the outer computational boundary. Schlamp¹⁷ placed it more than 1100 radii away, Nieuwstadt²⁰ placed it slightly more than 23 radii, while Underwood used only 4 radii at $Re = 10$. Takami and Keller¹⁸ used an extrapolation based on Imai's³² asymptotic solution of the Navier-Stokes equation. The procedure used by Hamielec and Raal is claimed by Keller³³ to be a modification of that set forth by Takami and himself.¹⁸ Keller disputes its validity.^{33,34}

The curve drawn through the data in Fig. 11 is an empirical result given by

$$(D/D_L) - 1 = -0.87\epsilon^2 + 0.154[1 - \exp(-Re)]\epsilon^3. \quad (21)$$

Equation (21) is simple in form and has only one adjustable constant. It is not unique, however. For $Re < 2$ the data can also be represented by $-0.87\epsilon^2 + 0.656\epsilon^3 + 0.113\epsilon^4$ or by $-0.87\epsilon^2 + 0.054\epsilon^4 - 0.52\epsilon^6$, for example. The theoretical formula of Skinner³¹ can be made to fit the data reasonably well (for $Re < 1.2$) by the addition of a term $0.4\epsilon^3$. All of these functions will diverge rapidly because of the singularity in ϵ at $Re \approx 7.4$. A fit based on a hyperbola displaced along the x-axis is $D/D_L - 1 = -0.1291[(Re + 0.3651)^2 - (0.3651)^2]^{1/2}$; this equation predicts to two decimals the

values of Schlamp¹⁷ but the curve shape is not quite right for $Re < 0.5$. This formula predicts also the values of Nieuwstadt and Keller at $Re = 10, 20, 30$ and 40 to the same accuracy.

Figure 12 is the traditional plot of drag coefficient versus Reynolds number. It compares the present work with Tritton's experimental values and with the formulas of Lamb and Kaplun. On the average, the present values are lower than Tritton's. From Fig. 12 it can be seen that Eq. (21) is limited in its range of prediction to $Re < 3$; above $Re = 3$ it diverges rapidly. Figure 13 shows $\log(C/\epsilon)$ plotted versus $\log(Re)$. On this type of plot Lamb's formula is a straight line with slope negative one. The asymptotic approach to Lamb's solution appears very clearly here.

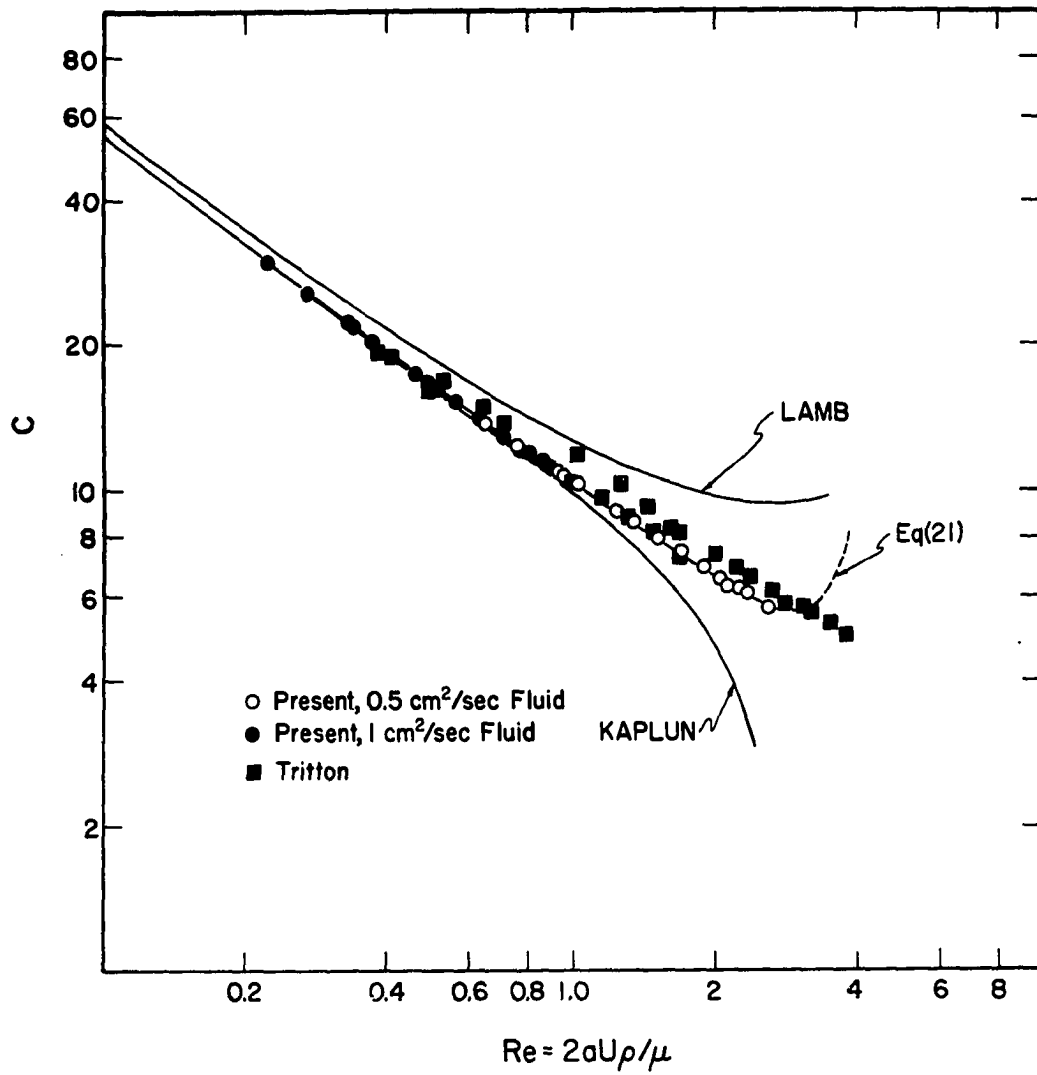


Fig. 12

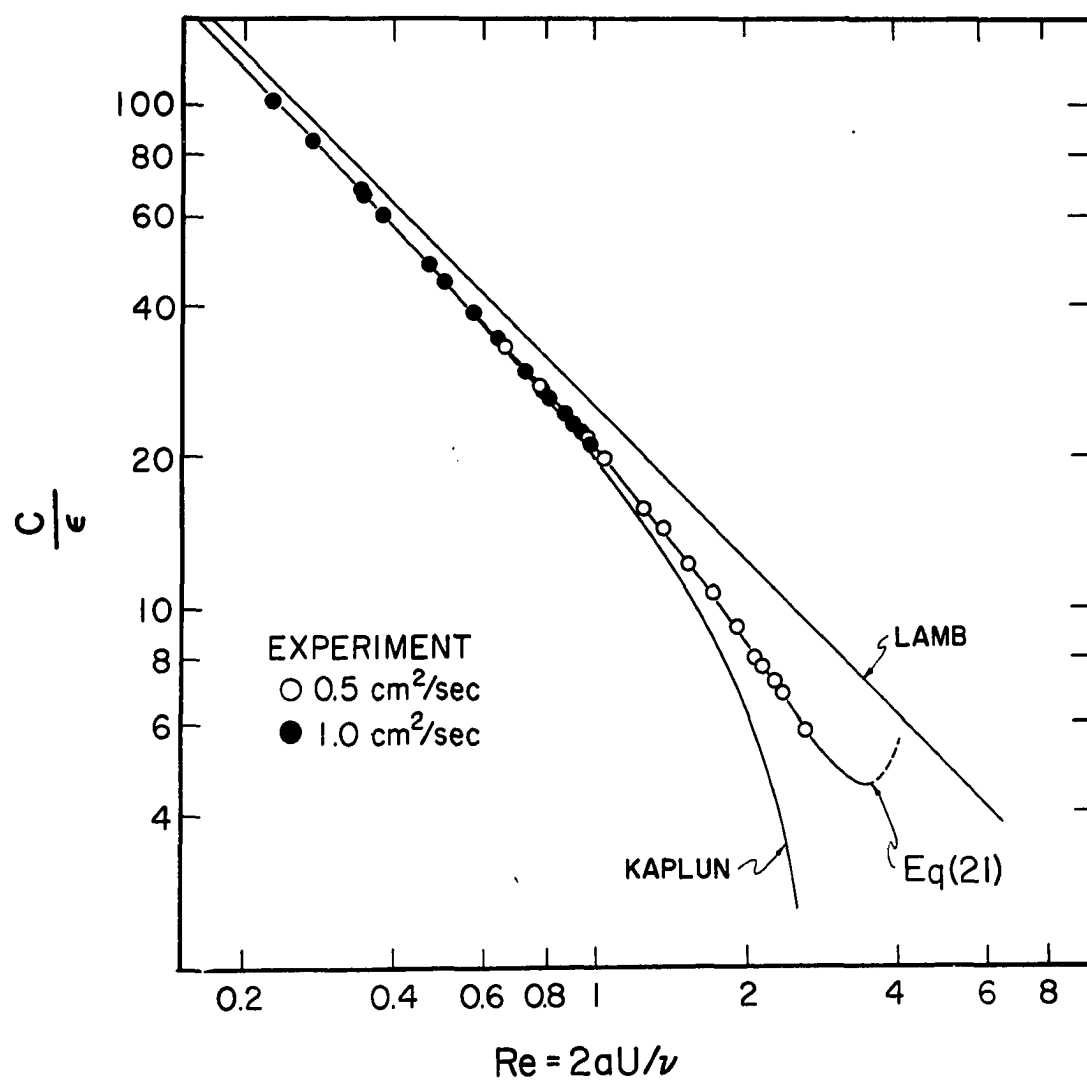


Fig. 13

CHAPTER IV

SUMMARY AND CONCLUSIONS

This experiment has provided experimental values of the drag per unit length of infinite length cylinders in an unbounded fluid. These values were deduced by empirical means from observations of the sedimentation of solitary, finite length cylinders in a large container. Since the intent of this experiment was to provide accurate values for the drag, care was taken to minimize the experimental uncertainties.

The drag was measured as the cylinder's effective weight in the fluid instead of indirectly calculating it because the direct measurement suppressed errors in the cylinder diameter, the cylinder length and the fluid density. This was particularly important for the smallest cylinder diameters used. The sedimentation velocity was measured by the time of flight method. For the experimental arrangement (Fig. 6) times of flight were reproducible to 0.1% and the velocity was calculated to an accuracy of 0.2%. Table III summarizes the error estimates.

The effects of finite boundaries and finite lengths were accounted for by empirical means. The container effects were primarily due to the sidewalls and were found to be small. Equation (15) yields corrections of less than 0.1%. The largest correction was due to the finite lengths of the

cylinders. A linear relation was observed between the reciprocal of the terminal velocity and the reciprocal of the cylinder's length (Fig. 9). This observation is qualitatively supported by Shi's low Reynolds number calculation for the transverse drag experienced by an ellipsoid of revolution. Extrapolations to infinite length caused corrections of 1.4% to 6.6% in the terminal velocity.

The results of this experiment (Fig. 11) and the previous sphere results (Fig. 4), when viewed together, indicate that the method of matched asymptotic expansions is a valid way of generating higher order corrections to the Lamb and Stokes solutions for the cylinder and the sphere respectively. The convergence of the method appears to be slow, however. Proudman³⁵ has suggested an alternate procedure for the sphere. Van Dyke's semianalytical method of series truncation seems to be a good way of extending the range of the analytical approximations. This is because the method solves a set of coupled ordinary differential equations. The mathematical treatment of ordinary differential equations is better understood than that of partial differential equations. Schlamp, et al., and Takami and Keller do show that good results can be predicted by solving partial differential equations, but care must be taken with the outer computational boundary. Finally, the present results approach the Lamb drag via Kaplun's formula implying that the Lamb drag is valid only at very small Reynolds numbers.

REFERENCES

1. G. G. Stokes, Trans. Cambr. Phil. Soc. 8, 287 (1845).
2. M. Van Dyke, Perturbation Methods in Fluid Mechanics (The Parabolic Press, Stanford, California, 1975)
Annotated ed. p. 152.
3. C. W. Oseen, Hydrodynamik. Leipzig: Akademische Verlag, 1927.
4. H. Lamb, Phil Mag. 21, 112 (1911).
5. I. Proudman and J. R. A. Pearson, J. Fluid Mech. 2, 237 (1957).
6. S. Kaplun, J. Math. Mech. 6, 595 (1957).
7. H. Schlichting, Boundary Layer Theory (McGraw-Hill, New York, 1968), 6th English ed., p. 16.
8. T. Maxworthy, J. Fluid Mech. 23, 369 (1965).
9. W. Chester and D. R. Breach, J. Fluid Mech. 37, 751 (1969).
10. S. C. R. Dennis and J. D. A. Walker, J. Fluid Mech. 48, 771 (1971).
11. M. Van Dyke, Proceedings 11th Inter. Congress of Appl. Mech., edited by H. Gortler, (Springer-Verlag, Berlin, 1966), p. 1165.
12. J. Lloyd Sutterby, Trans. Soc. Rheol. 17, 559 (1973).
13. R. L. Underwood, J. Fluid Mech. 37, 95 (1969).
14. R. E. Williams and R. G. Hussey, Phys. Fluids 15, 2083 (1972).

15. D. J. Tritton, J. Fluid Mech. 6, 547 (1959).
16. K. O. L. F. Jayaweera and B. J. Mason, J. Fluid Mech. 22, 709 (1964).
17. R. J. Schlamp, H. R. Pruppacher, and A. E. Hamielec, J. Atmos. Sci. 32, 2330 (1975).
18. H. Takami and H. B. Keller, Phys. Fluids Suppl. 12, II-51 (1969); see also H. B. Keller and H. Takami in Numerical Solutions of Nonlinear Differential Equations, edited by D. Greenspan (John Wiley & Sons, Inc., New York, 1966), p. 115, and H. B. Keller, Phys. Fluids 13, 533 (1970).
19. S. C. R. Dennis and M. Shimshoni, Great Britain Aero. Res. Council, Current Papers, No. 797 (1964); see also Ref. 17.
20. F. Nieuwstadt and H. B. Keller, Comput. Fluids 1, 59 (1973).
21. A. E. Hamielec and J. D. Raal, Phys. Fluids 12, 11 (1969); see also Ref. 17.
22. F. O. Griffin, M. S. Thesis, Department of Chem. Eng., University of British Columbia, Vancouver, Canada; see also Ref. 17.
23. R. E. Williams, Ph.D. Thesis, Department of Physics and Astronomy, Louisiana State University, Baton Rouge, Louisiana.
24. C. C. Currie and B. F. Smith, Ind. Eng. Chem. 42, 2457 (1950).

25. R. S. Marvin, J. Res. Natl. Bur. Std. (U.S.) 75A, 535 (1971).
26. C. M. White, Proc. Roy. Soc. (London) A186, 472 (1946).
27. Y. Takaisi, J. Phys. Soc. Japan 10, 685 (1955).
28. N. J. deMestre, J. Fluid Mech. 58, 641 (1973).
29. H. Brenner, J. Fluid Mech. 12, 35 (1962).
30. Yun-Yuan Shi, J. Fluid Mech. 23, 657 (1965).
31. L. A. Skinner, Quart. J. Mech. Appl. Math. 28, 333 (1975); see also Ref. 2, pp. 234-238.
32. I. Imai, Proc. Roy. Soc., London, Ser. A, 208, 487 (1951).
33. H. B. Keller, Phys. Fluids 13, 533 (1969).
34. A. E. Hamielec and J. D. Raai, Phys. Fluids 13, 534 (1969).
35. See Ref. 9.

VITA

Burke Huner was born March 22, 1948 in Baton Rouge, Louisiana. His primary and secondary educations were received in the East Baton Rouge Parish public school system and he was graduated from Robert E. Lee High School, Baton Rouge, Louisiana in 1966. A Bachelor of Science in Physics was awarded at Louisiana State University in 1970 and a Master of Science in Physics was awarded in 1972 also from L.S.U. He is presently a candidate for the degree of Doctor of Philosophy in the Department of Physics and Astronomy.

EXAMINATION AND THESIS REPORT

Candidate: Burke Huner

Major Field: Physics

Title of Thesis: Cylinder Drag at Low Reynolds Number

Approved:

R.D. Hussey

Major Professor and Chairman

James B. Ingham

Dean of the Graduate School

EXAMINING COMMITTEE:

John T. Marshall

L. H. Teetsworth

Marshall

Claude J. Givins

Date of Examination:

July 20, 1977